

Rotating Concentric Circular Peakons

Darryl D. Holm

Theoretical Division and Center for Nonlinear Studies
Los Alamos National Laboratory, MS B284
Los Alamos, NM 87545
email: dholm@lanl.gov

Mathematics Department

Imperial College of Science, Technology and Medicine
London SW7 2AZ, UK
email: d.holm@imperial.ac.uk

Vakhtang Putkaradze

Department of Mathematics and Statistics
University of New Mexico Albuquerque, NM 87131-1141
email: putkarad@math.unm.edu

and

Samuel N. Stechmann

Theoretical Division and Center for Nonlinear Studies
Los Alamos National Laboratory, MS B284
Los Alamos, NM 87545
email: sam@t7.lanl.gov

Courant Institute of Mathematical Sciences

New York University
New York, NY 10012
email: stechman@cims.nyu.edu

November 9, 2018

Abstract

We study invariant manifolds of measure-valued solutions of the partial differential equation for geodesic flow of a pressureless fluid. These solutions describe interaction dynamics on lower-dimensional support sets; for example, curves, or filaments, of momentum in the plane. The 2+1 solutions we study are planar generalizations of the 1+1 peakon solutions of Camassa & Holm [1993] for shallow water solitons. As an example, we study the canonical Hamiltonian interaction dynamics of N rotating concentric circles of peakons, whose solution manifold is $2N$ -dimensional. Thus, the problem is reduced from infinite dimensions to a finite-dimensional, canonical, invariant manifold. The existence of this reduced solution manifold and many of its properties may be understood, by noticing that it is also the momentum map for the action of diffeomorphisms on the space of curves in the plane. We show both analytical and numerical results.

PACS numbers: 47.35, 11.10.Ef, 45.20.Jj

Keywords: Shallow water flows, Hamiltonian systems, Momentum filaments.

Contents

1	Introduction and overview	3
2	Measure-valued momentum maps and solutions of geodesic flow in n dimensions	
3	Lie-Poisson bracket for rotating concentric circles of peakons	11
4	Azimuthally symmetric peakons	13
4.1	Derivation of equations	13
4.2	Solution properties	16
5	Numerical Results for Radial Peakons	17
5.1	Radial peakon collisions	17
5.2	Bouncing off the center	20
6	Numerical Results for Rotating Peakon Circles	21
7	Conclusions	26

1 Introduction and overview

Geodesic flow in n dimensions

As first shown in Arnold [1966] [1], Euler's equations of ideal fluid dynamics represent geodesic motion on the volume-preserving diffeomorphisms with respect to the the L^2 norm of the velocity. More generally, a time-dependent smooth map $g(t)$ is a geodesic on the diffeomorphisms with respect to a kinetic energy norm $KE = \frac{1}{2}\|\mathbf{u}\|^2$, provided its velocity, the right-invariant tangent vector $\mathbf{u} = \dot{g}g^{-1}(t)$, satisfies the **vector Euler-Poincaré equation**,

$$\partial_t \mathbf{m} = -\mathbf{u} \cdot \nabla \mathbf{m} - \nabla \mathbf{u}^T \cdot \mathbf{m} - \mathbf{m} \operatorname{div} \mathbf{u} \equiv -\operatorname{ad}_{\mathbf{u}}^* \mathbf{m}. \quad (1)$$

Here ad^* is the adjoint with respect to L^2 pairing $\langle \cdot, \cdot \rangle : \mathfrak{g}^* \times \mathfrak{g} \rightarrow \mathbb{R}$ of the ad-action (commutator) of vector fields $\mathbf{u}, \mathbf{w} \in \mathfrak{g}$. That is,

$$\langle \operatorname{ad}_{\mathbf{u}}^* \mathbf{m}, \mathbf{w} \rangle = -\langle \mathbf{m}, \operatorname{ad}_{\mathbf{u}} \mathbf{w} \rangle = -\langle \mathbf{m}, [\mathbf{u}, \mathbf{w}] \rangle. \quad (2)$$

The momentum vector $\mathbf{m} \in \mathfrak{g}^*$ is defined as the variational derivative of kinetic energy with respect to velocity,

$$\delta(KE) = \langle \mathbf{m}, \delta \mathbf{u} \rangle \Leftrightarrow \mathbf{m} = \frac{\delta(KE)}{\delta \mathbf{u}}. \quad (3)$$

This defining relation for momentum closes the Euler-Poincaré equation (1) for geodesic motion with respect to the kinetic energy metric $KE = \frac{1}{2}\|\mathbf{u}\|^2$. For more details, extensions and applications of the Euler-Poincaré equation to both compressible and incompressible fluid and plasma dynamics, see Holm, Marsden and Ratiu [1998] [12].

Geodesic flow with H^1 velocities in two dimensions

In this paper, we consider the *solution behavior* of the Euler-Poincaré equation (1) when the momentum vector is related to the velocity by the two-dimensional Helmholtz operation,

$$\mathbf{m} = \mathbf{u} - \Delta \mathbf{u}, \quad (4)$$

where Δ denotes the Laplacian operator. This Helmholtz relation arises when the kinetic energy is given by the H^1 norm of the velocity,

$$KE = \frac{1}{2} \|\mathbf{u}\|_{H^1}^2 = \frac{1}{2} \int |\mathbf{u}|^2 + |\nabla \mathbf{u}|^2 dx dy. \quad (5)$$

The H^1 kinetic energy norm (5) is an approximation of the Lagrangian in Hamilton's principle for columnar motion of shallow water over a flat bottom, when potential energy is negligible (the zero linear dispersion limit) and the kinetic energy of vertical motion is approximated by the second term in the integral, [3]. In this approximation, the physical meaning of the quantity $\mathbf{m} = \delta(KE)/\delta\mathbf{u}$ in the Helmholtz relation (4) is the momentum of the shallow water flow, while \mathbf{u} is its velocity in two dimensions. See Kruse et al. [2001] [4] for details of the derivation of the geodesic equation for approximating 2D shallow water dynamics in this limit.

Problem statement: Geodesic flow on H^1 in cylindrical symmetry

The present work studies azimuthally symmetric solutions of the Euler-Poincaré equation (1) in polar coordinates (r, ϕ) ,

$$\mathbf{m} = m_r(r, t) \hat{\mathbf{r}} + m_\phi(r, t) \hat{\phi} \quad \text{and} \quad \mathbf{u} = u_r(r, t) \hat{\mathbf{r}} + u_\phi(r, t) \hat{\phi}. \quad (6)$$

In the standard basis for cylindrical coordinates, momentum one-forms and velocity vector fields are expressed as,

$$\mathbf{m} \cdot d\mathbf{x} = m_r dr + rm_\phi d\phi \quad \text{and} \quad \mathbf{u} \cdot \nabla = u_r \partial_r + \frac{u_\phi}{r} \partial_\phi. \quad (7)$$

Solutions (6) satisfy coupled partial differential equations whose radial and azimuthal components are, respectively,

$$\frac{\partial m_r}{\partial t} = -\frac{1}{r} \partial_r (rm_r u_r) - m_r \partial_r u_r - (rm_\phi) \partial_r \left(\frac{u_\phi}{r} \right), \quad (8)$$

$$\frac{\partial (rm_\phi)}{\partial t} = -\frac{1}{r} \partial_r (r^2 m_\phi u_r). \quad (9)$$

In these coupled equations, nonzero rotation u_ϕ generates radial velocity u_r , which influences the azimuthal motion. Without rotation, $u_\phi = 0$, and the solution becomes purely radial. The system of equations (8) and (9) for geodesic motion conserves the H^1 kinetic energy norm,

$$KE([u_r], [u_\phi]) = \frac{1}{2} \int \left[u_\phi^2 + u_{\phi,r}^2 + \frac{u_\phi^2}{r^2} + u_r^2 + u_{r,r}^2 + \frac{u_r^2}{r^2} \right] r dr = \frac{1}{2} \|\mathbf{u}\|_{H^1}^2. \quad (10)$$

The corresponding momenta satisfy the dual relations,

$$rm_\phi = \frac{\delta KE}{\delta(u_\phi/r)} \quad \text{and} \quad m_r = \frac{\delta KE}{\delta u_r}. \quad (11)$$

The Helmholtz relation (4), between m_ϕ and u_ϕ , for example, becomes

$$m_\phi = u_\phi - \frac{\partial^2 u_\phi}{\partial r^2} - \frac{1}{r} \frac{\partial u_\phi}{\partial r} + \frac{1}{r^2} u_\phi = \left(1 - \frac{1}{r} \partial_r r \partial_r + \frac{1}{r^2}\right) u_\phi. \quad (12)$$

This relation between velocity and momentum defines the symmetric invertible Helmholtz operator in cylindrical geometry with finite boundary conditions at $r = 0$ and $\rightarrow \infty$. The velocity $u(r, t)$ is obtained from the momentum $m(r, t)$ by the convolution $u(r) = G * m = \int_0^\infty G(r, \xi) m(\xi) \xi d\xi$ (an extra factor ξ arises in cylindrical geometry) with the Green's function $G(r, \xi)$. The Green's function for the radial Helmholtz operator in (12) is given by,

$$G(r, \xi) = \begin{cases} I_1(\xi) K_1(r) & \text{for } \xi < r, \\ I_1(r) K_1(\xi) & \text{for } r < \xi, \end{cases} \quad (13)$$

where I_1 and K_1 are modified Bessel's functions. This Green's function will play a significant role in what follows.

Equations (8) and (9) may be written equivalently as a Hamiltonian system, by Legendre transforming the kinetic energy $KE([u_r], [u_\phi])$ to the Hamiltonian $h([m_r], [rm_\phi])$, after which the equations take the form,

$$\frac{\partial}{\partial t} \begin{bmatrix} m_r \\ rm_\phi \end{bmatrix} = \begin{bmatrix} \{m_r, h\} \\ \{rm_\phi, h\} \end{bmatrix} = -\mathcal{D} \begin{bmatrix} \delta h / \delta m_r \\ \delta h / \delta (rm_\phi) \end{bmatrix} = -\mathcal{D} \begin{bmatrix} u_r \\ u_\phi/r \end{bmatrix}, \quad (14)$$

where $\delta h / \delta m_r = u_r$, $\delta h / \delta (rm_\phi) = u_\phi/r$ and the Hamiltonian operator \mathcal{D} ,

$$\mathcal{D} = \begin{bmatrix} r^{-1} \partial_r rm_r + m_r \partial_r & rm_\phi \partial_r \\ r^{-1} \partial_r r^2 m_\phi & 0 \end{bmatrix}, \quad (15)$$

is the matrix $\mathcal{D} = \{(m_r, rm_\phi), (m_r, rm_\phi)\}$, which defines the Lie-Poisson bracket for geodesic motion in cylindrical geometry. Note that \mathcal{D} is skew-symmetric with respect to the L^2 pairing with cylindrical radial measure.

2 Measure-valued momentum maps and solutions of geodesic flow in n dimensions

Measure-valued solution ansatz

Based on the peakon solutions for the Camassa-Holm equation [2] and its generalizations to include the other traveling-wave pulson shapes [8], Holm & Staley [9] introduced the following measure-valued ansatz for the solutions of the vector EP equation (1),

$$\mathbf{m}(\mathbf{x}, t) = \sum_{a=1}^N \int_s^N \mathbf{P}^a(s, t) \delta(\mathbf{x} - \mathbf{Q}^a(s, t)) ds, \quad \mathbf{m} \in \mathbb{R}^n, \quad s \in \mathbb{R}^k, \quad (16)$$

where the dimensions satisfy $k < n$. The fluid velocity corresponding to the momentum solution ansatz (16) is given by

$$\mathbf{u}(\mathbf{x}, t) = G * \mathbf{m} = \sum_{b=1}^N \int_{s'}^N \mathbf{P}^b(s', t) G(\mathbf{x}, \mathbf{Q}^b(s', t)) ds', \quad \mathbf{u} \in \mathbb{R}^n, \quad (17)$$

where $G(\mathbf{x}, \mathbf{y})$ is the Green's function for the Helmholtz operator in n dimensions. These solutions are vector-valued functions whose momenta are supported in \mathbb{R}^n on a set of N surfaces (or curves) of codimension $(n - k)$ for $s \in \mathbb{R}^k$ with $k < n$. In three dimensions, for example, they may be supported on sets of points (vector peakons, $k = 0$), quasi one-dimensional filaments (strings, $k = 1$), or quasi two-dimensional surfaces (sheets, $k = 2$). Substitution of the solution ansatz (16) into the EP equation (1) implies the following integro-partial-differential equations (IPDEs) for the evolution of such strings, or sheets,

$$\begin{aligned} \frac{\partial}{\partial t} \mathbf{Q}^a(s, t) &= \sum_{b=1}^N \int_{s'}^N \mathbf{P}^b(s', t) G(\mathbf{Q}^a(s, t), \mathbf{Q}^b(s', t)) ds', \\ \frac{\partial}{\partial t} \mathbf{P}^a(s, t) &= - \sum_{b=1}^N \int_{s'}^N (\mathbf{P}^a(s, t) \cdot \mathbf{P}^b(s', t)) \frac{\partial}{\partial \mathbf{Q}^a(s, t)} G(\mathbf{Q}^a(s, t), \mathbf{Q}^b(s', t)) ds'. \end{aligned} \quad (18)$$

Importantly for the interpretation of these solutions given later in Holm and Marsden [2003] [11], the independent variables $s \in \mathbb{R}^k$ turn out to be

Lagrangian coordinates. When evaluated along the curve $\mathbf{x} = \mathbf{Q}^a(s, t)$, the fluid velocity (17) satisfies,

$$\mathbf{u}(\mathbf{x}, t) \Big|_{\mathbf{x}=\mathbf{Q}^a(s,t)} = \sum_{b=1}^N \int_{s'} \mathbf{P}^b(s', t) G(\mathbf{Q}^a(s, t), \mathbf{Q}^b(s', t)) ds' = \frac{\partial \mathbf{Q}^a(s, t)}{\partial t}. \quad (19)$$

Consequently, the lower-dimensional support sets (defined on $\mathbf{x} = \mathbf{Q}^a(s, t)$ and parameterized by coordinates $s \in \mathbb{R}^k$) move with the fluid velocity. Moreover, equations (18) for the evolution of these support sets are canonical Hamiltonian equations,

$$\frac{\partial}{\partial t} \mathbf{Q}^a(s, t) = \frac{\delta H_N}{\delta \mathbf{P}^a}, \quad \frac{\partial}{\partial t} \mathbf{P}^a(s, t) = -\frac{\delta H_N}{\delta \mathbf{Q}^a}. \quad (20)$$

The corresponding Hamiltonian function $H_N : (\mathbb{R}^n \times \mathbb{R}^n)^{\otimes N} \rightarrow \mathbb{R}$ is,

$$H_N = \frac{1}{2} \int_s \int_{s'_a} \sum_{b=1}^N (\mathbf{P}^a(s, t) \cdot \mathbf{P}^b(s', t)) G(\mathbf{Q}^a(s, t), \mathbf{Q}^b(s', t)) ds ds'. \quad (21)$$

This is the Hamiltonian for canonical geodesic motion on the cotangent bundle of a set of N curves $\mathbf{Q}^a(s, t)$, $a = 1, \dots, N$, with respect to the metric given by G .

Hamiltonian geodesic dynamics under the measure-valued vector solution ansatz (16) for the EP equation (1) was investigated numerically in Holm & Staley [2003b] [10]. We refer to that paper for more details of the solution dynamics.

The non-locality of the dynamics of the measured-valued solutions, described in the literature, makes analytical progress difficult. In this paper, we derive measured-valued solutions that are rotationally symmetric. For this circular symmetry, the non-locality integrates out and the motion reduces to a set of ordinary differential equations. Most of the paper is devoted to these circular solutions, which we call rotating peakons. The set of solutions obeying translational symmetry, but having two velocity components, is studied in the appendix. For a solution of N planar peakons, there are $2N$ degrees of freedom, with $2N$ positions and $2N$ canonically conjugate momenta. Hence, evolution of the N planar peakon solution is governed by a set of $4N$ nonlocal partial differential equations. These reduce to ordinary differential equations in the presence of either rotational, or translational symmetry. We also demonstrate that these solutions emerge from any initial condition with this symmetry in the plane.

Potential applications of measure-valued solutions of geodesic flow

One of the potential applications of the two-dimensional version of this problem involves the internal waves on the interface between two layers of different density in the ocean. Fig. 1 shows a striking agreement between two internal wave trains propagating at the interface of different density levels in the South China Sea, and the solution appearing in the simulations of the EP equation (1) in two dimensions. Inspired by this figure, we shall construct a theory of propagating one-dimensional momentum filaments in two dimensions. For other work on the 2D CH equation in the context of shallow water waves, see Kruse, et al. (2001) [4].

Another potential application of the two-dimensional version of this problem occurs in image processing for computational anatomy, e.g., brain mapping from PET scans. For this application, one envisions the geodesic motion as an optimization problem whose solution maps one measured two-dimensional PET scan to another, by interpolation in three dimensions along a geodesic path between them in the space of diffeomorphisms. In this situation, the measure-valued solutions of geodesic flow studied here correspond to “cartoon” outlines of PET scan images. The geodesic “evolution” in the space between them provides a three dimensional image that is optimal for the chosen norm. For a review of this imaging approach, which is called “template matching” in computational anatomy, see Miller and Younes [2002] [13].

Peakon Momentum Map $J : T^*S \rightarrow \mathfrak{g}^*$ in n dimensions

Holm and Marsden [2003] [11] explained an important component of the general theory underlying the remarkable reduced solutions of the vector EP equation (1). In particular, Holm and Marsden [2003] [11] showed that the solution ansatz (16) for the momentum vector in the EP equation (1) introduced in Holm and Staley [2003] [10] defines a **momentum map** for the action of diffeomorphisms on the support sets \mathcal{S} of the Dirac delta functions. These support sets are points on the real line for the CH shallow water equation in one dimension. They are points, curves, or surfaces in \mathbb{R}^n for the vector EP equation (1) in n -dimensions.

Momentum map definition. Let a group G act on a manifold S , and lift the action of G to the cotangent bundle T^*S . A momentum map J is a Poisson map from T^*S to \mathfrak{g}^* , the dual of the Lie algebra of G . (A

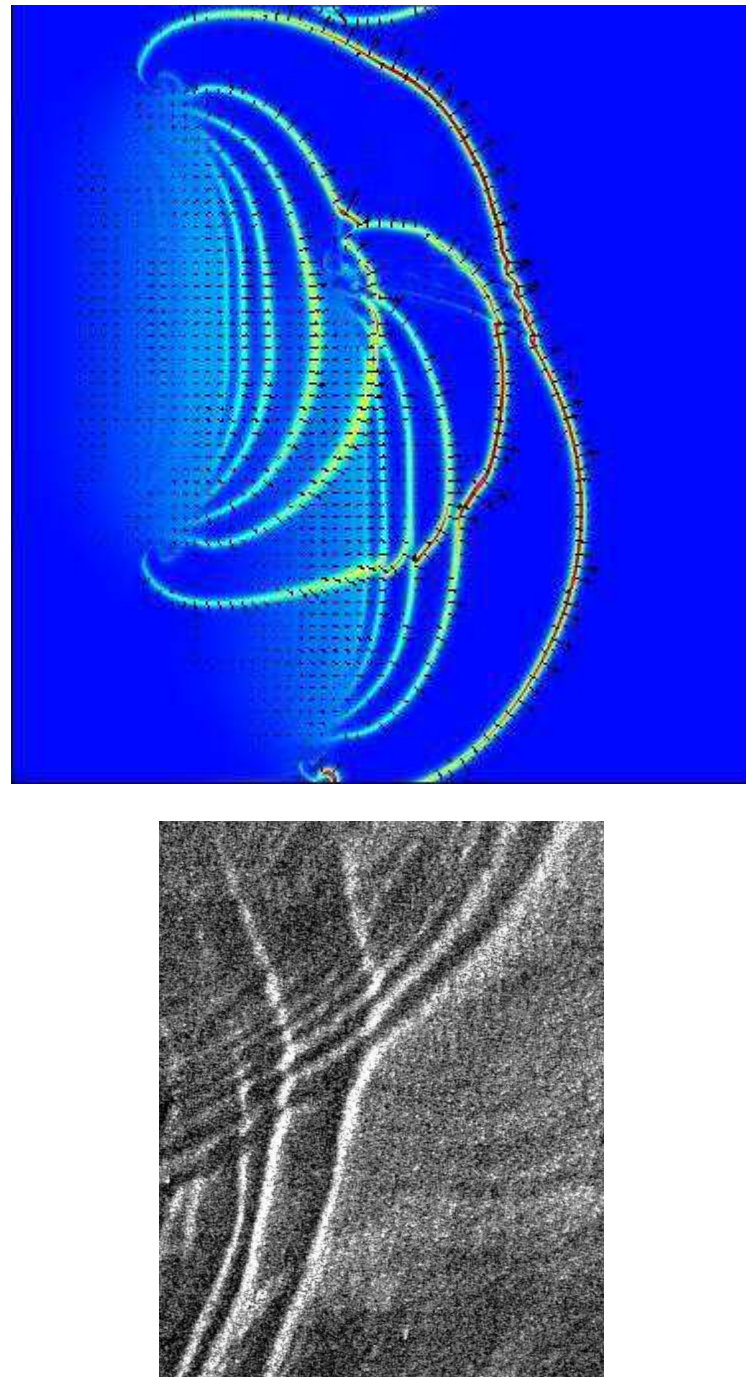


Figure 1: Simulation of the full EP equation (1), courtesy of Martin Staley (top). Internal waves in the South China Sea (bottom).

map is Poisson, provided it is coadjoint equivariant. In particular, J maps the canonical Poisson bracket on the image space T^*S into the Lie-Poisson bracket on the target space \mathfrak{g}^* .) In symbols, this is

$$\begin{aligned} J : (\mathbf{P}, \mathbf{Q}) \in T^*S &\longrightarrow \mathbf{m} \in \mathfrak{g}^*, \\ J : \{f, h\}_{can}(\mathbf{P}, \mathbf{Q}) &\longrightarrow \{f, h\}_{LP}(\mathbf{m}) = \left\langle \mathbf{m}, \left[\frac{\delta f}{\delta \mathbf{m}}, \frac{\delta h}{\delta \mathbf{m}} \right] \right\rangle, \\ \text{where } \langle \cdot, \cdot \rangle : \mathfrak{g}^* \times \mathfrak{g} &\longrightarrow \mathbb{R}. \end{aligned}$$

The n -dimensional peakon momentum solution ansatz J (for any Hamiltonian) is given by Holm and Staley [2003] [10] as the superposition formula in (16),

$$J : \mathbf{m}(\mathbf{x}, t) = \sum_{a=1}^N \int_s \mathbf{P}^a(s, t) \delta(\mathbf{x} - \mathbf{Q}^a(s, t)) ds, \quad \mathbf{m} \in \mathbb{R}^n, \quad s \in \mathbb{R}^k. \quad (22)$$

By direct substitution using the canonical \mathbf{Q}, \mathbf{P} Poisson brackets, one computes the Poisson property of the map J in n Cartesian dimensions. Namely,

$$\{m_i(\mathbf{x}), m_j(\mathbf{y})\}_{can}(\mathbf{P}, \mathbf{Q}) = - \left(\frac{\partial}{\partial x^j} m_i(\mathbf{x}) + m_j(\mathbf{x}) \frac{\partial}{\partial x^i} \right) \delta(\mathbf{x} - \mathbf{y}), \quad (23)$$

in the sense of distributions integrated against a pair of smooth functions of \mathbf{x} and \mathbf{y} . This expression defines the Lie-Poisson bracket $\{\cdot, \cdot\}_{LP}(\mathbf{m})$ defined on the dual Lie algebra \mathfrak{g}^* , restricted to momentum filaments supported on the N curves $\mathbf{x} = \mathbf{Q}^a(s, t)$, where $a = 1, 2, \dots, N$. Its calculation demonstrates the following.

Theorem 2.1 (*Holm and Marsden [2003]*) *The momentum solution ansatz (16), for measure-valued solutions of the vector EP equation (1), is a momentum map.*

The Poisson property of the momentum map J in (22) is, of course, independent of the choice of Hamiltonian. This independence explains, for example, why the map extends from peakons of a particular shape, to the pulsions of any shape studied in Fringer and Holm [2001] [8]. The solution ansatz (16) now rewritten as the momentum map J in (22) is also a Lagrange-to-Euler map, because the momentum is supported on filaments that *move with the fluid velocity*. Hence, the motion governed by the vector EP equation (1) occurs by the action of the diffeomorphisms in G on the support set of the

fluid momentum, whose position and *canonical* momentum are defined on the cotangent bundle T^*S of the space of curves S . This observation informs the study of geodesic motion governed by equation (1). For complete details and definitions, see Holm and Marsden [2003] [11].

Peakon momentum map $J : T^*S \rightarrow \mathfrak{g}^*$ on a Riemannian manifold

The goal of the present work is to characterize the measure-valued solutions of the vector EP equation (1), by using the momentum map J in (22) when S is the space of concentric circles in the plane. The motion and interactions of these measure-valued solutions may be either purely radial (circles of peakons), or they may also have an azimuthal component (rotating circles of peakons). To accomplish this goal, we employ a result from Holm and Staley [2003b] [10] that on a Riemannian manifold M with metric determinant $\det g(\mathbf{x})$, the measure-valued momentum ansatz (16) becomes

$$\mathbf{m}(\mathbf{x}, t) = \sum_{a=1}^N \int_s \mathbf{P}^a(s, t) \frac{\delta(\mathbf{x} - \mathbf{Q}^a(s, t))}{\sqrt{\det g}} ds, \quad \mathbf{m} \in M, \quad s \in \mathbb{R}^k. \quad (24)$$

This solution ansatz is also a momentum map, as shown in Holm and Marsden [2003] [11]. On a Riemannian manifold, the corresponding Lie-Poisson bracket for the momentum on its support set becomes

$$\{m_i(\mathbf{x}), m_j(\mathbf{y})\} = - \left(m_j(\mathbf{x}) \frac{\partial}{\partial x^i} + \frac{1}{\sqrt{\det g}} \frac{\partial}{\partial x^j} \sqrt{\det g} m_i(\mathbf{x}) \right) \frac{\delta(\mathbf{x} - \mathbf{y})}{\sqrt{\det g}}. \quad (25)$$

For example, in cylindrical symmetry one has $\sqrt{\det g} = r$ and the vector \mathbf{m} depends only on the radial coordinate r . For solutions with these symmetries, the Lagrangian label coordinate s is unnecessary, as we shall see in the cylindrical case, and the equations for \mathbf{Q}^a and \mathbf{P}^a will reduce to ordinary differential equations in time.

3 Lie-Poisson bracket for rotating concentric circles of peakons

Azimuthal relabeling symmetry for rotating circular peakons

We shall consider the dynamics of circles of peakons, whose motion may have both radial and azimuthal components. These are rotating circular

peakons. Suppose one were to mark a Lagrangian point on the a -th circle, $a = 1, \dots, N$. Then the change in its azimuthal angle $\phi_a(t)$ could be measured as it moved with the azimuthal fluid velocity u_ϕ along the the a -th circle as its radius $r = q_a(t)$ evolved. Translations in the Lagrangian azimuthal coordinate would shift the mark, but this shift of a Lagrangian label would have no effect on the Eulerian velocity dynamics of the system. Such a Lagrangian relabeling would be a symmetry for any Hamiltonian depending only on Eulerian velocity. Thus, the azimuthal relabeling would result in the conservation of its canonically conjugate angular momentum M_a , which generates the rotation corresponding to the relabeling symmetry of the a -th circle. The a -th circle would be characterized in phase space by its radius $r = q_a(t)$, and its canonically conjugate radial momentum, denoted as p_a . The rotational degree of freedom of the a -th circle would be represented by its conserved angular momentum M_a and its ignorable canonical azimuthal angle ϕ_a . The only nonzero canonical Poisson brackets among these variables are,

$$\{q_a, p_b\}_{can} = \delta_{ab} \quad \text{and} \quad \{\phi_a, M_b\}_{can} = \delta_{ab}. \quad (26)$$

Momentum map for rotating circular peakons

In terms of their $4N$ canonical phase space variables (q_a, p_a, ϕ_a, M_a) , with $a = 1, 2, \dots, N$, the superposition formula (22) for N rotating circular peakons may be expressed as,

$$\mathcal{J}: \mathbf{m}(r, t) = \sum_{a=1}^N \left(p_a(t) \hat{\mathbf{r}} + \frac{M_a}{q_a(t)} \hat{\phi} \right) \frac{\delta(r - q_a(t))}{r}. \quad (27)$$

We shall first verify that this formula is a momentum map, and then in section 4 we shall derive it, by requiring it to be a valid solution ansatz for the geodesic EP equation (1) in polar coordinates. As a consequence, the motion governed by the system of partial differential equations (8) and (9) for geodesic motion in the plane with azimuthal symmetry has a finite dimensional invariant manifold in the $2N$ -dimensional canonical phase space (q_a, p_a) for each choice of the N angular momentum values M_a , with $a = 1, 2, \dots, N$. Later, we shall also examine numerical studies of these solutions when the kinetic energy is chosen to be the H^1 norm of the azimuthally symmetric fluid velocity.

By direct substitution using the canonical Poisson brackets in (26), one computes the Poisson property of the map \mathcal{J} in (27). Namely,

$$\begin{aligned} \{m_r(r), m_r(r')\}_{can}(\mathbf{p}, \mathbf{q}) &= -\left(\frac{1}{r} \frac{\partial}{\partial r} r m_r(r) + m_r(r) \frac{\partial}{\partial r}\right) \frac{\delta(r-r')}{r}, \\ \{m_r(r), r' m_\phi(r')\}_{can}(\mathbf{p}, \mathbf{q}) &= -r m_\phi(r) \frac{\partial}{\partial r} \frac{\delta(r-r')}{r}, \\ \{r m_\phi(r), m_r(r')\}_{can}(\mathbf{p}, \mathbf{q}) &= -\frac{1}{r} \frac{\partial}{\partial r} r^2 m_\phi(r) \frac{\delta(r-r')}{r}, \\ \{r m_\phi(r), r m_\phi(r')\}_{can}(\mathbf{p}, \mathbf{q}) &= 0. \end{aligned} \quad (28)$$

These equalities are written in the sense of distributions integrated against a pair of smooth functions of r and r' . They demonstrate the Poisson property of the map \mathcal{J} in (27), which is also the solution ansatz for the rotating circular peakons. They also express the Lie-Poisson bracket $\{\cdot, \cdot\}_{LP}(m_r, r m_\phi)$ for momentum filaments defined on the dual Lie algebra \mathfrak{g}^* and restricted to the support set of these solutions. Hence, we have demonstrated the following:

Proposition 3.1 *The map \mathcal{J} in (27) is a momentum map.*

On comparing the formulas in (28) with the Hamiltonian operator \mathcal{D} for the continuous solutions in (15), one sees that the momentum map (27) essentially restricts the Lie-Poisson bracket with Hamiltonian operator \mathcal{D} to its support set. Next, we shall derive the momentum map (27) by requiring it to be a valid solution ansatz for the geodesic EP equation (1) in polar coordinates.

4 Azimuthally symmetric peakons

4.1 Derivation of equations

We seek azimuthally symmetric solutions of the geodesic EP equation (1) in polar coordinates (r, ϕ) , for which

$$\mathbf{m} = m_r(r, t) \hat{\mathbf{r}} + m_\phi(r, t) \hat{\phi} \equiv (m_r(r, t), m_\phi(r, t)). \quad (29)$$

We shall derive the momentum map (27) and the canonical Hamiltonian equations for its parameters (q_a, p_a, M_a) by assuming solutions in the form,

$$\mathbf{m}(r, t) = \sum_{i=1}^N \left(p_i(t) \hat{\mathbf{r}} + v_i(t) \hat{\phi} \right) \frac{\delta(r - q_i(t))}{r}. \quad (30)$$

These solutions represent concentric cylindrical momentum filaments which are rotating around the origin. The corresponding velocity components are obtained from

$$(u_r(r, t), u_\phi(r, t)) = \int r' G(r, r') (m_r(r', t), m_\phi(r', t)) dr', \quad (31)$$

where $G(r, r') = G(r', r)$ is the (symmetric) Green's function for the radial Helmholtz operator given in formula (13). Hence, the fluid velocity corresponding to the solution ansatz (30) assumes the form,

$$\mathbf{u}(r, t) = \sum_{j=1}^N \left(p_j(t) \hat{\mathbf{r}} + v_j(t) \hat{\phi} \right) G(r, q_j(t)), \quad (32)$$

with Green's function $G(r, q_j(t))$ as in formula (13). In addition, the kinetic energy of the system is given by

$$KE(\mathbf{p}, \mathbf{q}, \mathbf{v}) = \frac{1}{2} \int \mathbf{u} \cdot \mathbf{m} r dr = \frac{1}{2} \sum_{i,j=1}^N \left(p_i p_j + v_i v_j \right) G(q_i, q_j). \quad (33)$$

Substitution of the solution ansatz (30) for the momentum and its corresponding velocity (32) into the radial equation (8) gives the system,

$$\begin{aligned} & \sum_i \left(\dot{p}_i \frac{\delta(r - q_i)}{r} - p_i \dot{q}_i \frac{\delta'(r - q_i)}{r} \right) \\ & + \sum_{i,j} \left\{ p_i p_j G(r, q_j) \left[-\frac{\delta(r - q_i)}{r^2} + \frac{\delta'(r - q_i)}{r} \right] + 2p_i p_j \frac{\delta(r - q_i)}{r} \frac{\partial G}{\partial r}(r, q_j) \right. \\ & \quad \left. + (p_i p_j - v_i v_j) \frac{\delta(r - q_i)}{r^2} G(r, q_j) + v_i v_j \frac{\delta(r - q_i)}{r} \frac{\partial G}{\partial r}(r, q_j) \right\} = 0. \end{aligned}$$

Multiplying this system by the smooth test function $r\psi(r)$ and integrating with respect to r yields dynamical equations for p_i and q_i . In particular, the $\psi(q_i)$ terms yield

$$\dot{p}_i = - \sum_j \left(p_i p_j \frac{\partial G}{\partial q_i} + v_i v_j \left\{ \frac{\partial G(q_i, q_j)}{\partial q_i} - \frac{G(q_i, q_j)}{q_i} \right\} \right), \quad (34)$$

and, after integrating by parts, the $\psi'(q_i)$ terms yield

$$\dot{q}_i = \sum_j p_j G(q_i, q_j). \quad (35)$$

By equation (32) we see that $\dot{q}_i(t) = \hat{\mathbf{r}} \cdot \mathbf{u}(q_i, t)$, so the radius of the i -th cylinder moves with the radial velocity of the flow.

This procedure is repeated for the ϕ component of the EP equation, by substituting the solution ansatz (30,32) into equation (9), to find the system

$$\begin{aligned} & \sum_i \left(\dot{v}_i \frac{\delta(r - q_i)}{r} - v_i \dot{q}_i \frac{\delta'(r - q_i)}{r} \right) \\ & + \sum_{i,j} \left\{ v_i p_j G(r, q_j) \left[-\frac{\delta(r - q_i)}{r^2} + \frac{\delta'(r - q_i)}{r} \right] \right. \\ & \left. + v_i p_j \frac{\delta(r - q_i)}{r} \left(\frac{\partial G}{\partial r}(r, q_j) + 2 \frac{G(r, q_j)}{r} \right) \right\} = 0. \end{aligned}$$

Upon multiplying this system by $r\psi(r)$ and integrating with respect to r , the term proportional to $\psi'(q_i)$ again recovers exactly the q_i -equation (35). The term proportional to $\psi(q_i)$ gives

$$\dot{v}_i = - \frac{v_i}{q_i} \sum_j p_j G(q_i, q_j) = - v_i \frac{\dot{q}_i}{q_i}, \quad (36)$$

after using the q_i -equation (35) in the last step. This integrates to

$$v_i q_i = M_i = \text{const}, \quad (37)$$

where M_i are N integration constants. From the Hamiltonian viewpoint, this was expected: The angular momentum M_i is conserved for each individual circular peakon, because each circle may be rotated independently without changing the energy.

Equations (34) and (35) for p_i and q_i may now be recognized as Hamilton's canonical equations with Hamiltonian,

$$H(\mathbf{p}, \mathbf{q}, \mathbf{M}) = \frac{1}{2} \int \mathbf{u} \cdot \mathbf{m} r dr = \frac{1}{2} \sum_{i,j=1}^N \left(p_i p_j + \frac{M_i M_j}{q_i q_j} \right) G(q_i, q_j). \quad (38)$$

This is the same Hamiltonian as obtained from substituting the momentum map (27) into the kinetic energy KE in equation (33). Hence, we may recover the reduced equations (34) for p_i , (35) for q_i and (37) for M_i from the Hamiltonian (38) and the canonical equations,

$$\dot{p}_i = -\frac{\partial H}{\partial q_i}, \quad \dot{q}_i = \frac{\partial H}{\partial p_i}, \quad \dot{M}_i = -\frac{\partial H}{\partial \phi_i} = 0. \quad (39)$$

This result proves the following:

Proposition 4.1 *The momentum map (27) is a valid ansatz for rotating peakon solutions of the Euler-Poincaré equation (1) for geodesic motion.*

4.2 Solution properties

The remaining canonical equation for the i -th Lagrangian angular frequency is,

$$\dot{\phi}_i = \frac{\partial H}{\partial M_i} = \sum_j \frac{M_j}{q_i q_j} G(q_i, q_j) = \frac{1}{q_i} \sum_j v_j(t) G(q_i, q_j). \quad (40)$$

Thus, as expected, the ignorable canonical angle variables $\phi = \{\phi_i\}$, with $i = 1, 2, \dots, N$, decouple from the other Hamiltonian equations. In addition, we see that

$$q_i \dot{\phi}_i(t) = \hat{\phi} \cdot \mathbf{u}(q_i, t), \quad (41)$$

so the angular velocity of the i -th cylinder *also* matches the angular velocity of the flow. Therefore, we have shown:

Proposition 4.2 *The canonical Hamiltonian parameters in the momentum map and solution ansatz (27) provide a Lagrangian description in cylindrical symmetry of the flow governed by the Eulerian EP equation for geodesic motion (1).*

Angular momentum, fluid circulation and collapse to the center. Finally, the fluid circulation of the i -th concentric circle c_i , which is traveling with velocity \mathbf{u} , may be computed from equations (29) and (30) (with a slight abuse of notation) as,

$$\oint_{c_i(\mathbf{u})} \mathbf{m} \cdot d\mathbf{x} = \oint_{c_i(\mathbf{u})} r m_\phi d\phi = 2\pi v_i = \frac{2\pi M_i}{q_i}. \quad (42)$$

We see that the “angular velocity” $v_i = M_i/q_i$ is the fluid circulation of the i -th concentric circle. Since the angular momentum M_i of the i -th circle is conserved, its circulation $v_i(t)$ varies inversely with its radius. Consequently, this circulation would diverge, if the i -th circle were to collapse to the center with nonzero angular momentum.

5 Numerical Results for Radial Peakons

5.1 Radial peakon collisions

We consider purely radial solutions of equation (8), with $m_\phi = 0$, which satisfy

$$\frac{\partial m_r}{\partial t} = -\frac{1}{r}\partial_r(r m_r u_r) - m_r \partial_r u_r. \quad (43)$$

Such radial solutions have no azimuthal velocity. Without azimuthal velocity, the vector peakon solution ansatz (30) for momentum reduces to the scalar relation,

$$m_r(r, t) = \sum_{i=1}^N p_i(t) \frac{\delta(r - q_i(t))}{r}. \quad (44)$$

The corresponding radial velocity is

$$u_r(r, t) = \sum_{i=1}^N p_i(t) G(r, q_i(t)), \quad (45)$$

where the Green’s function $G(r, q_i(t))$ for the radial Helmholtz operator is given by formula (13). Radial peakons of this form turn out to be the building blocks for the solution of any radially symmetric initial value problem. We have found numerically that the initial value problem for equation (44) with any initially confined radial distribution of velocity quickly splits up into radial peakons. This behavior is illustrated in Fig. 2. The initial distribution of velocity splits almost immediately into a train of radial peakons arranged by height, or, equivalently, speed.

The head-on “peakon-antipeakon” collisions are of special interest. In the case of equal strength radial peakon-antipeakon collisions, the solution appears to develop infinite slope in finite time, see Fig. 3. This behavior is

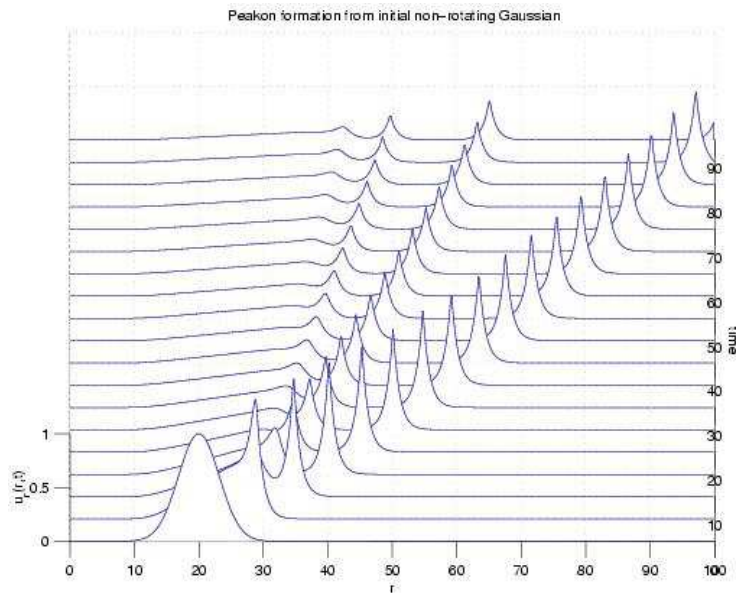


Figure 2: The initial value problem: a Gaussian profile splits into peakons.

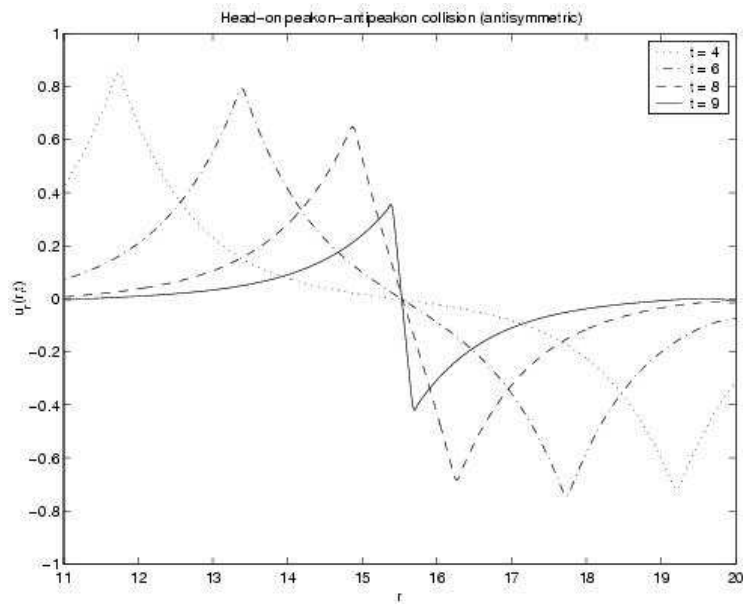


Figure 3: Peakon-antipeakon collision of equal strength.

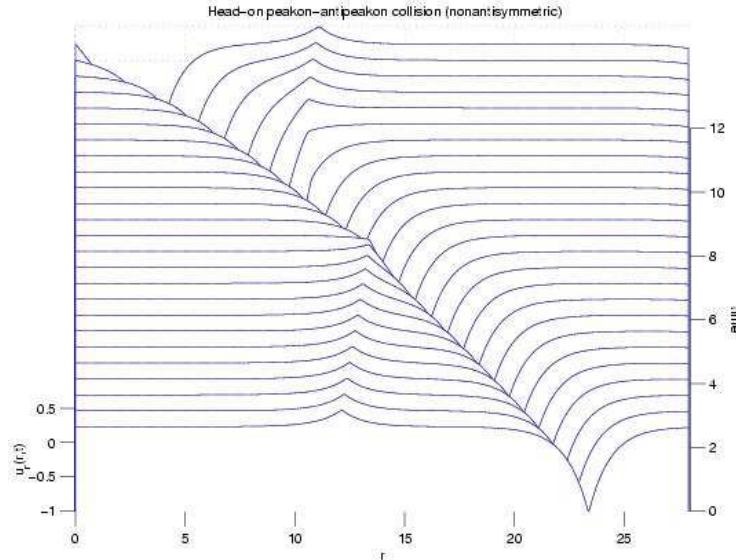


Figure 4: Peakon-antipeakon collision of unequal strength. The smaller peakon's trajectory undergoes a large phase shift.

also known to occur for peakon-antipeakon collisions on the real line. If the strengths of the peakon and antipeakon are not equal, then the larger one of them seems to ‘plow’ right through the smaller one. This is shown in Fig. 4.

The figures shown were produced from numerical simulations of the Eulerian PDE (43). The momentum m_r was advanced in time using a fourth-order Runge-Kutta method. The time step was chosen to ensure the Hamiltonian $\frac{1}{2} \int \mathbf{m} \cdot \mathbf{u} r dr$ was conserved to within 0.1% of its initial value. The spatial discretizations ranged from $dr = 10^{-4}$ to $dr = 0.02$ depending on the desired resolution and the length of the spatial domain, and the spatial derivatives were calculated using finite differences. Fourth- and fifth-order centered differencing schemes were used for the first and second derivatives, respectively. The momentum m_r was found from the velocity u_r using the finite difference form of the radial Helmholtz operator, and the velocity u_r was found from the momentum m_r by inverting the radial Helmholtz matrix. For the peakon interaction simulations, the initial conditions were given by a sum of peakons of the form (45) for some chosen initial p_i and q_i . For a peakon collapsing to the center, which will be described next, the boundary condition at the origin is important. If the PDE (43) were extended to $r < 0$, then the velocity

would be an *odd* function about the origin. In addition, when the peakon was sufficiently close to the origin ($q_i < 0.1$), the sign of its momentum m_r was reversed to begin its expansion away from the origin.

For comparison with the simulations of the Eulerian PDE (43), simulations of the Lagrangian ODEs (39) were also performed. A fourth-order Runge-Kutta method was used to advance the system in time, and a time step was chosen to ensure the Hamiltonian (38) was conserved to within 0.1%. The results of these simulations agreed with those of the Eulerian PDE simulations to within 1%.

5.2 Bouncing off the center

Let us first consider the case when only one peakon collapses onto the center with the angular momentum being zero. The Hamiltonian in this case is,

$$H = \frac{1}{2}p^2 I_1(q) K_1(q),$$

which can be approximated when $q \rightarrow 0$ as

$$H = \left(\frac{1}{4} + o(q) \right) p^2.$$

Thus, the momentum $p(t)$ is nearly constant just before the collapse time, t_* , and is approximately equal to $-2\sqrt{H}$, more precisely,

$$p = -2\sqrt{H} + o(q).$$

The equation of motion for $q(t)$ yields, $\dot{q} = p I_1(q) K_1(q) = -\sqrt{H} + o(q)$. If $q \rightarrow 0$ at $t \rightarrow t_*$, then we necessarily have

$$q(t) = \sqrt{H}(t_* - t) + o((t_* - t)^2),$$

near the time of collapse $t \rightarrow t_*$.

The case of N radial peakons can be considered similarly. If only one peakon (let us say, number a) collapses into the center at time t_* , so $q_a(t) \rightarrow 0$ as $t \rightarrow t_*$, and the motion of the peakons away from the center is regular in some interval $(t_* - \delta, t_* + \delta)$ (as will be the case unless a peakon-antipeakon collision occurs during this interval), then conservation of the Hamiltonian implies

$$p_a^2 G(q_a, q_a) + 2p_a A + B = 2H, \quad (46)$$

where

$$A = \sum_{i \neq a} p_i G(q_a, q_i),$$

$$B = \sum_{(i,j) \neq a} p_i p_j G(q_i, q_j)$$

Since $q_a = \min(q_1, \dots, q_N)$, the Helmholtz Green's function in expression (13) implies that the quantities A and B are bounded at times close to t_* , and that $G(q_a, q_a)$ is bounded as well. Consequently, equation (46) implies that p_a is also bounded at times close to $t = t_*$.

Numerical simulations confirm our predictions: At the moment of the impact at the center, the amplitude of the peakon remains bounded and approaches the value of $-\sqrt{H} \approx -2.23$, as illustrated on Fig. 5.

The slope of the solution at the origin has to diverge. This can be seen on the example of a single peakon as follows. Since

$$\frac{\partial u}{\partial r} \big|_{r=0} = p(t) I'_1(0) K_1(q) = \frac{1 + o(q)}{2} \frac{p(t)}{q(t)}$$

Thus, if $q(t) \rightarrow 0$ as $t \rightarrow t_*$, the slope $\partial_r u(r = 0, t)$ must diverge. Therefore, the following Proposition is true:

Proposition 5.1 *A radially symmetric peakon with no angular momentum, collapsing to the center, has bounded momentum and unbounded slope at the origin close to the moment of collapse.*

6 Numerical Results for Rotating Peakon Circles

Simulations of rotating peakons were performed for the Eulerian system of PDEs (8,9) using the same numerical methods as those used for non-rotating peakons. Fig. 6 shows the results of an initial value problem simulation when u_r is initially 0 and u_ϕ is initially a Gaussian function. Radial velocity in both directions is almost immediately generated, and rotating peakons soon emerge moving both inward and outward but all rotating in the same direction. A rotating peakon approaches the center but turns around before reaching the origin.

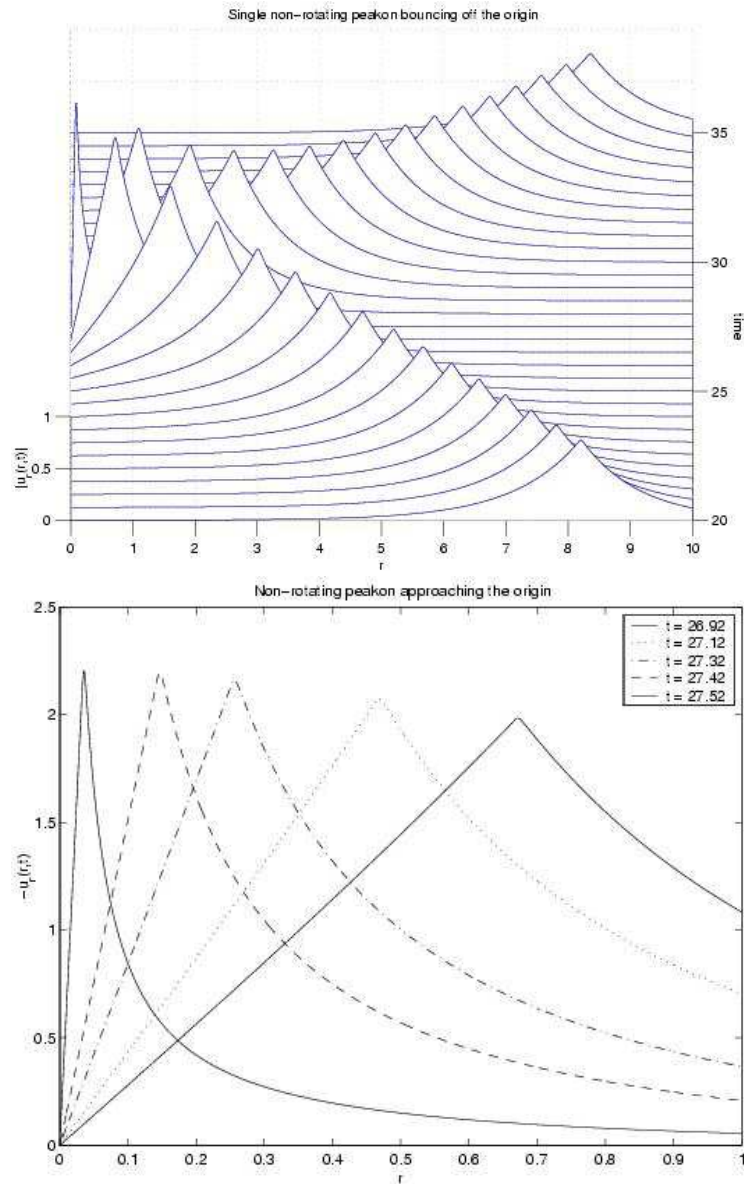


Figure 5: Impact of a peakon onto the center.

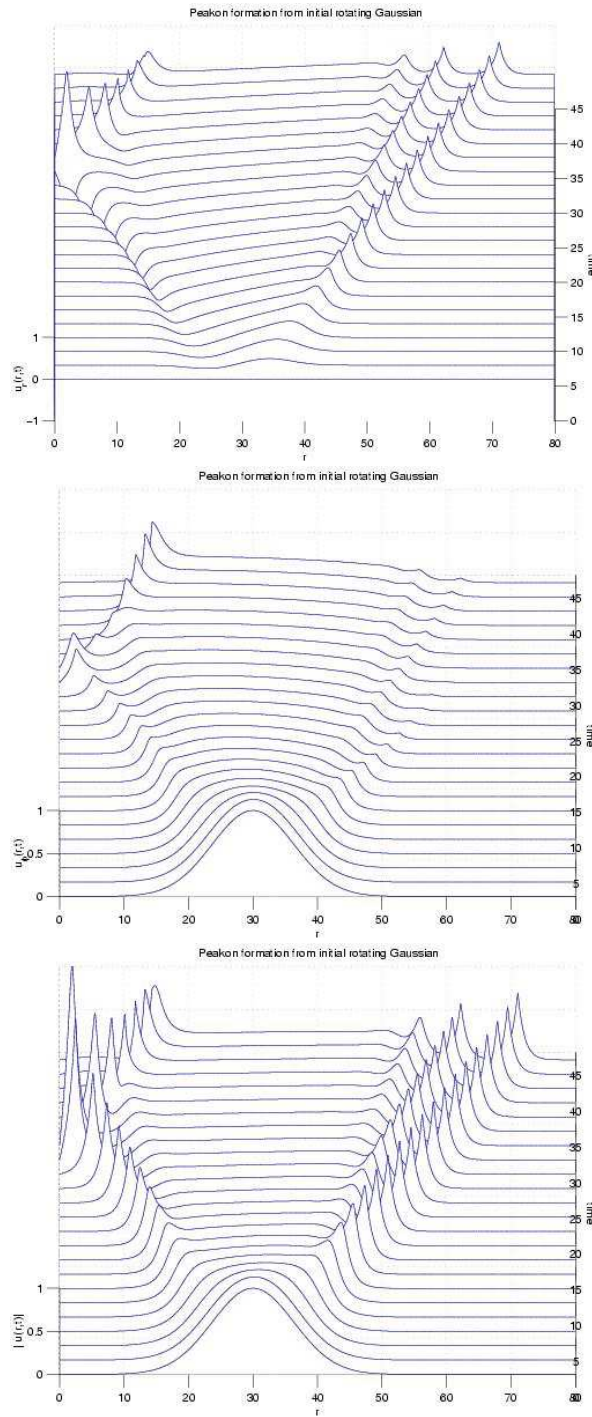


Figure 6: An initial angular velocity distribution (with zero initial radial velocity) breaks up into rotating peakons which move both inward and outward. The radial velocity u_r , the angular velocity u_ϕ , and the velocity magnitude $|\mathbf{u}|$ are all shown.

Fig. 7 shows a rotating peakon as it approaches the origin. A sort of angular momentum barrier is reached, and the peakon turns around and moves away from the origin. Thus, a peakon's behavior as it approaches the origin is reminiscent of Sundman's Theorem; if a peakon has nonzero angular momentum, then a full collapse to the origin will not occur. This result can be understood as follows. For a single rotating peakon, the Hamiltonian (38) becomes

$$H = \left(p^2 + \frac{M^2}{q^2} \right) G(q, q)$$

From the theory of Bessel functions we know that $G(q, q) \rightarrow 1/2$ when $q \rightarrow 0$, and $G(q, q) > 0$ for all q . Moreover, it can be shown that $G(q, q)$ is strictly decreasing with increasing $q > 0$, so we conclude that $G(q, q) > G(q_0, q_0)$ if $0 < q < q_0$. Thus, when $0 < q < q_0$,

$$H \geq \frac{M^2}{q^2} G(q_0, q_0)$$

so

$$q \geq \max \left(q_0, M \sqrt{\frac{G(q_0, q_0)}{H}} \right) \quad (47)$$

The estimate (47) provides the lower bound $q(t)$ can reach in the process of evolution for each value of the parameter q_0 . This estimate can be further optimized as follows. Since $G(q_0, q_0)$ is strictly decreasing starting with the value of $G(0, 0) = 1/2$, there is $q_*(M, H)$ such that

$$q_* = M \sqrt{\frac{G(q_*, q_*)}{H}} \quad (48)$$

for each value of $M, H > 0$. Then, $q \geq q_*(M, H)$ is the desired optimal estimate. We can summarize this result in

Proposition 6.1 *Consider a rotating radial peakon with given values $M, H > 0$. If we define $q_*(M, H)$ by (48), then in the process of evolution this peakon cannot be closer than $q_*(M, H)$ to the origin.*

Note One can show that $q_*(M, H) \sim M/\sqrt{2H} + O(M^3)$ for $M \rightarrow 0$.

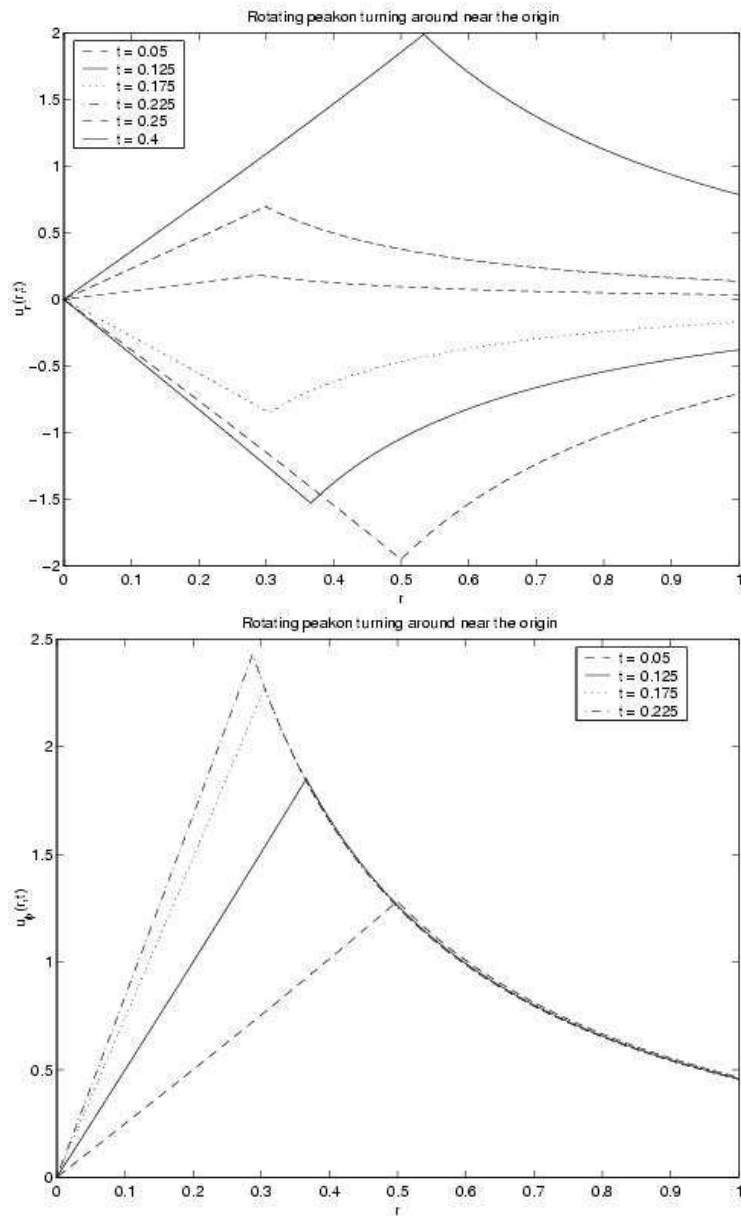


Figure 7: A rotating peakon turns around near the origin. The radial velocity changes sign as the angular velocity reaches a maximum.

7 Conclusions

The momentum map (16) for the action of diffeomorphisms on (closed) curves in the plane was used to generate invariant manifolds of measure-valued solutions of the Euler-Poincaré equation (1) for geodesic motion on the diffeomorphism group. The H^1 norm of the fluid velocity was chosen for the kinetic energy of a class of solutions whose momentum support set was a family of N closed curves arranged as concentric circles on the plane. These finite-dimensional invariant manifolds of cylindrically symmetric solutions generalized the N -peakon (soliton) solutions of the Camassa-Holm equation from motion of points along the real line, to motion with cylindrical symmetry. This cylindrical motion included rotation, or, equivalently, circulation, which drives the radial motion. The momentum map with non-zero circulation for these concentric circles yielded a generalization of the circular CH peakons that included their rotational degrees of freedom. The canonical Hamiltonian parameters in the momentum map *and* solution ansatz (27) for the concentric rotating circular peakons provided a finite-dimensional Lagrangian description in cylindrical symmetry of the flow governed by the Eulerian EP partial differential equation for geodesic motion (1). Numerically, we studied the basic interactions of these circular peakons amongst themselves, by collisions and by collapse to the center, with and without rotation.

The main conclusions from our numerical study were:

- Collapse to the center without rotation occurs with bounded canonical momentum and with vertical radial slope in velocity at $r = 0$, at the instant of collapse.
- For nonzero rotation, collapse to the center cannot occur and the slope at $r = 0$ never becomes infinite.

The main questions that remain are:

- Numerical simulations show that near vertical or vertical slope occurs at head-on collision between two peakons of nearly equal height. A rigorous proof of this fact is still missing.
- Is the motion integrable on our $2N$ dimensional Hamiltonian manifold of concentric rotating circular peakons for any $N > 1$ and any choice of Green's function?

- How does one determine the number and speeds of the rotating circular peakons that emerge from a given initial condition?
- How does the momentum map with internal degrees of freedom generalize to n dimensions?

All of these challenging problems are beyond the scope of the present paper and will be the subjects of future work.

Acknowledgements

We are enormously grateful to our friends and colleagues for their scientific suggestions and help during the course of this work. We are especially grateful to Martin Staley for his help and cooperation in producing first class numerics for Figure 1. We are also grateful for support and hospitality. D.D.H. is grateful for support by US DOE, from contract W-7405-ENG-36 and from US DOE, Office of Science ASCAR/MICS. V. P. acknowledges the hospitality of the Los Alamos National Laboratory and Center for Nonlinear Studies, where he was able to spend one day a week during academic year 2002-2003. V. P. was partially supported by Petroleum Foundation Research Grant Number 40218-AC9. S. S. acknowledges summer student support at the Theoretical Division at Los Alamos National Laboratory.

References

- [1] V.I. Arnold, Sur la géométrie différentielle des groupes de Lie de dimension infinie et ses applications à l'hydrodynamique des fluids parfaits. *Ann. Inst. Fourier, Grenoble* **16** (1966) 319-361.
- [2] R. Camassa and D. D. Holm, An Integrable Shallow Water Equation with Peaked Solitons. *Phys. Rev. Lett.* **71**, 1661-1664 (1993).
- [3] R. Camassa, D. D. Holm and C.D. Levermore, Long-Time Effects of Bottom Topography in Shallow Water. *Physica D*, **98** (1996) 258-286.
- [4] H. P. Kruse, J. Schreule and W. Du, A two-dimensional version of the CH equation. In *Symmetry and Perturbation Theory: SPT 2001* Edited by D. Bambusi, G. Gaeta and M. Cadoni. World Scientific: New York, pp 120-127 (2001).

- [5] A. Degasperis, D. D. Holm and A. N. W. Hone, A new integrable equation with peakon solutions. *Theoret. and Math. Phys.* **133**, 1463-1474 (2002).
- [6] H. R. Dullin, G. Gottwald and D. D. Holm, An integrable shallow water equation with linear and nonlinear dispersion. *Phys. Rev. Lett.*, **87**, no.19, (2001) 194501-04.
- [7] H. R. Dullin, G. Gottwald and D. D. Holm, Camassa-Holm, Korteweg-de Vries-5 and other asymptotically equivalent equations for shallow water waves. *Fluid Dyn. Res.* **33** (2003) 73-95
- [8] O. Fringer and D. D. Holm, Integrable vs nonintegrable geodesic soliton behavior. *Physica D* **150** (2001) 237-263.
- [9] D. D. Holm and M. F. Staley, Nonlinear balance and exchange of stability in dynamics of solitons, peakons, ramps/cliffs and leftons in a 1+1 nonlinear evolutionary pde. *Phys. Lett. A* **308**, 437-444 (2003).
- [10] D. D. Holm and M. F. Staley, Wave Structures and Nonlinear Balances in a Family of Evolutionary PDEs. To appear in *SIADS*.
- [11] D. D. Holm and J. E. Marsden, Momentum Map for Measure-valued Solutions (Peakons, Filaments and Sheets) for Geodesic Motion in n Dimensions. *Fest-Schrift Proceedings for Alan Weinstein*, Springer 2003. To appear
- [12] D. D. Holm, J. E. Marsden and T. S. Ratiu, The Euler–Poincaré equations and semidirect products with applications to continuum theories. *Adv. in Math.*, **137** (1998) 1-81.
- [13] M. I. Miller and L. Younes, Group Actions, Homeomorphisms, and Matching: A General Framework. *International Journal of Computer Vision* **41** (2001) 61-84.

8 Appendix: Extension of one-dimensional peakons

In this appendix, we show how to obtain the momentum line peakons, which are generalizaion of the line peakons. The standard ansatz for the regular

one-dimensional peakon is

$$m(x, t) = \sum_{i=1}^N p_i(t) \delta(x - q_i(t)), \quad (49)$$

where m satisfies the one-dimensional version of (1). We propose the following extension of these solutions:

$$\mathbf{m}(x, t) = \sum_{i=1}^N (p_i(t) \hat{\mathbf{x}} + v_i(t) \hat{\mathbf{y}}) \delta(x - q_i(t)), \quad (50)$$

where $\hat{\mathbf{x}}, \hat{\mathbf{y}}$ are unit vectors in x, y directions, respectively. The solution lives on line filaments, which are parallel to the y axis and propagate by translation along the x axis. However, the y component of momentum now has a non-trivial value. Such solutions represent momentum lines which propagate perpendicular to the shock's front and “slide” parallel to the front, moving surrounding ‘fluid’ with it. Upon substituting (50) into equations of motion (1), we see that the x and the y components of (1) both give the same equation of motion for $q_i(t)$:

$$\dot{q}_i(t) = \sum_j p_j G(q_i, q_j).$$

This compatibility is what makes the factorized solution (50) possible. The equation of motion for p_i is

$$\dot{p}_i(t) = \sum_j (p_i p_j + v_i v_j) G'(q_i, q_j),$$

and for v_i ,

$$\dot{v}_i = 0.$$

Thus, v_i can be considered as a set of parameters. The (p_i, q_i) still satisfy Hamilton's canonical equations, with Hamiltonian now given by,

$$H = \frac{1}{2} \sum_{i,j=1}^N (p_i p_j + v_i v_j) G(q_i, q_j). \quad (51)$$

Finally, the “angle” variables $y_i(t)$ conjugate to $v_i(t)$ with canonical Poisson bracket $\{y_i, v_j\} = \delta_{ij}$ satisfy:

$$\dot{y}_i(t) = \sum_j v_j G(q_i, q_j).$$